Journal of
PERIODONTAL RESEARCH

J Periodont Res 2013

JOURNAL OF PERIODONTAL RESEARCH
doi:10.1111/jre.12115

In vitro and *in vivo* characterization of porcine acellular dermal matrix for gingival augmentation procedures

A. M. Pabst[1], A. Happe[2], A. Callaway[3], T. Ziebart[1], S. I. Stratul[4], M. Ackermann[5], M. A. Konerding[5], B. Willershausen[3], A. Kasaj[3]

[1]Department of Oral and Maxillofacial Surgery, University Medical Center, Mainz, Germany, [2]Department of Oral and Maxillofacial Plastic Surgery, University of Cologne, Cologne, Germany, [3]Department of Operative Dentistry and Periodontology, University Medical Center, Mainz, Germany, [4]Department of Periodontology, Victor Babes University of Medicine and Pharmacology, Timisoara, Romania and [5]Institute of Functional and Clinical Anatomy, University Medical Center, Mainz, Germany

Pabst AM, Happe A, Callaway A, Ziebart T, Stratul SI, Ackermann M, Konerding MA, Willershausen B, Kasaj A. In vitro and in vivo characterization of porcine acellular dermal matrix for gingival augmentation procedures. J Periodont Res 2013; doi: 10.1111/jre.12115. © 2013 John Wiley & Sons A/S. Published by John Wiley & Sons Ltd

Background and Objective: Recently, porcine acellular dermal matrix (PADM) has been proposed as a possible alternative to autogenous grafts in periodontal plastic surgery. The aim of the present study was to investigate the *in vitro* responses of four different oral cell lines cultured on a novel PADM. Furthermore, tissue reaction to PADM was evaluated histologically after subcutaneous implantation in mice.

Material and Methods: Human gingival fibroblasts (HGF), human osteoblast-like cells, human umbilical vein endothelial cells and human oral keratinocytes (HOK) were cultured and transferred on to the PADM. A tissue culture polystyrene surface served as the control. The viability of all tested cell lines on PADM was measured by using the 3-(4,5-dimethylthiazol-2-yl)-2,5-diphenyl tetrazolium bromide colorimetric assay and PrestoBlue® reagent. The ToxiLight® assay was performed to analyze the effect of PADM on adenylate kinase release. PADM was implanted into nude mice subcutaneously and subjected to histological analysis after 21 d.

Results: Using 3-(4,5-dimethylthiazol-2-yl)-2,5-diphenyl tetrazolium bromide colorimetric assays, all tested cell lines cultured on PADM demonstrated a significant increase of viability compared to the control group (each $p < 0.001$) with the exception of HGF and HOK after 3 d (each $p > 0.05$). According to the PrestoBlue® analysis, all cell lines demonstrated a significant increase of viability compared to the control group at the particular points of measurement after 18 h (HGF $p < 0.01$; human osteoblast-like cells, human umbilical vein endothelial cells, HOK each $p < 0.001$). No significant cytotoxic effects of PADM on the tested cell lines could be observed, as assessed by changes in adenylate kinase release. Subcutaneous implantation of PADM into nude mice demonstrated good integration with surrounding tissues and significant revascularization of its collagen structure.

Conclusion: Overall, the results suggest that PADM is a promising substitute for autogenous soft tissue grafts in periodontal surgery.

Adrian Kasaj, DDS, PhD, Department of Operative Dentistry and Periodontology, Johannes Gutenberg-University Mainz, Augustusplatz 2, 55131 Mainz, Germany
Tel: +49 6 1311 73556
Fax: +49 6 1311 73406
e-mail: Kasaj@gmx.de

Key words: collagen; collagen matrix; graft; porcine acellular dermis; tissue regeneration

Accepted for publication May 18, 2013

Gingival recession and subsequent root surface exposure is a common occurrence and often requires treatment due to aesthetic concerns or root sensitivity (1). In recent years, a variety of surgical procedures have been proposed to obtain root coverage and increase the width of attached gingiva, including pedicle flaps such as coronally or laterally advanced flaps, free gingival grafts and subepithelial connective tissue grafts (CTG) (2). In terms of root coverage and gain in keratinized tissue, the CTG is the most predictable (3) procedure and considered the gold standard for root coverage care. However, major shortcomings of harvesting CTGs are patient morbidity associated with the second surgical site, as well as the limited supply of donor tissue for the treatment of multiple recession defects. For these reasons, a substitute for the autogenous donor tissue is desirable.

As a consequence, an acellular dermal matrix (ADM) allograft has been used as a CTG replacement in root coverage procedures. The ADM allograft is obtained from human cadaveric skin, which involves removal of the epidermal layer along with all cellular components without damaging the connective tissue matrix. This process leaves behind an extracellular collagenous matrix that provides the basis for cellular in-growth and subsequent tissue remodeling (4). A recent systematic review and meta-analysis, including eight clinical trials showed no statistically significant differences for any of the outcome measures (recession coverage, keratinized tissue formation, probing depths and clinical attachment levels) when comparing ADM versus CTG for root coverage procedures (5). However, the authors were unable to draw any definitive conclusion due to inadequate available data and emphasized the need for further research. Moreover, the use of human-based tissue products may be associated with ethical concerns and potential risk of disease transmission. Thus, most European countries have heavy restrictions on ADM allografts and its use has been limited. As a response, acellularized materials derived from xenogeneic sources have been introduced (6,7).

Recently, a new porcine-derived collagen matrix (mucoderm®, Botiss Dental, Berlin, Germany) has been approved as a soft tissue graft substitute and possible alternative to CTG and ADM in periodontal plastic surgery. Advantages of using porcine ADM (PADM) in place of cadaveric dermal matrices are in terms of avoiding the use of human donor tissue, its greater availability, low cost and ability to be harvested in large quantities. The PADM is processed to remove antigenic cellular components without causing any damage to the tissue structure and, thus, preserving the structural integrity of the entire extracellular collagenous matrix. It has been generally accepted that the intact extracellular collagenous matrix may act as a three-dimensional scaffold to allow in-growth and repopulation of fibroblasts, blood vessels and epithelium from surrounding tissues. Thus, with continuous production of new connective tissue and degradation of the original matrix, the material may become gradually replaced or incorporated by host tissues. However, the real value of this collagen matrix to allow repopulation of autogenous cells and its biological mechanism is still unknown.

The aim of the present study was to verify if PADM is a suitable three-dimensional matrix through its *in vitro* response to human gingival fibroblasts (HGF), human osteoblast-like (HOB) cells, human umbilical vein endothelial cells (HUVEC) and human oral keratinocytes (HOK). The potential of PADM to support cell viability *in vitro* was investigated. In addition, *in vivo* tissue reactions of PADM were tested histologically after subcutaneous implantation in mice.

Material and methods

Mucoderm® 3-dimensional collagen matrix

Mucoderm® is a pure porcine collagen tissue matrix without further artificial cross-linking or chemical treatment. The collagen matrix is derived from porcine dermis. The processing technique removes all antigenic components from the dermis, while maintaining the structure of the graft. The decellularization and sterilization process leaves behind a 3D matrix consisting of collagen and elastin. This 3D collagen matrix should facilitate cellular ingrowth from surrounding tissues and subsequent incorporation of the material into the newly formed tissue.

Scanning electron microscopy and interferometry 3-dimensional analysis

The matrices were hydrated in phosphate-buffered saline, dehydrated in ethanol, freeze-dried, cut and mounted on specimen holders, sputtered with gold in an argon atmosphere and visually examined using a Philips ESEM XL-30 scanning electron microscope (SEM; Philips, Eindhoven, Netherlands) at different magnifications. The matrix surface and morphology were examined with interferometry using a 3D digital microscope (VHX-2000, Keyence Corporation, Osaka, Japan) to characterize the roughness of the surface at the micrometer level.

Sample preparation

Even before the start of the *in vitro* and *in vivo* assays, discs of the mucoderm® matrix were prepared according to the manufacturer's instructions. The discs were created with a sterile, cylindrical, sharp surgical punch and the diameters of all samples (6 mm, $\pm$ 0.1 mm) were controlled with a sterile sliding caliper. Following that, the samples were hydrated in sterile 0.9% sodium chloride solution for 5 min. All procedures were performed under sterile conditions.

Cell culture

HGF (Lonza, Basel, Switzerland), HOB (PromoCell, Heidelberg, Germany), HUVEC (Lonza) and HOK (Provitro, Berlin, Germany) were used for the experiments. The cells were cultured in an incubator with 5% CO_2 and 95% air at 37°C.

Cells were passaged at regular intervals depending on their growth characteristics using 0.25% trypsin (Seromond Biochrom KG, Berlin, Germany).

HGF were grown in Stroma Cell Growth Medium (SCGM; Lonza) with 1% penicillin–streptomycin–neomycin antibiotic mixture, 10% fetal calf serum (FCS) and 1 ng/mL basic fibroblast growth factor.

HOB were grown in a solution composed of Dulbecco's modified Eagle's medium with 1% penicillin–streptomycin–neomycin antibiotic mixture, 1% L-glutamine and 10% FCS. Before the experiments, the osteoblasts were positively characterized by immunohistochemical expression of alkaline phosphatase and osteocalcin (labeled streptavidin–biotin/horseradish peroxidase).

HUVEC were cultured in an endothelial basal medium supplemented with 1 μg/mL hydrocortisone, 12 μg/mL bovine brain extract, 50 μg/mL gentamycin, 50 ng/mL amphotericin B, 10 ng/mL epidermal growth factor and 10% FCS.

HOK were cultured in keratinocyte growth medium (Provitro, Berlin, Germany). The medium contained 1 ng/mL fibroblast growth factor, 1 ng/mL epidermal growth factor, Ca^{2+} < 0.1 mM, insulin, without bovine pituitary extract and without hydrocortisone.

Cell morphology

Cell morphology and distribution of HGF on the mucoderm® matrix were assayed by direct fluorescence at 24 h, 5 d and 14 d. To demonstrate the cell morphology, adherence, proliferation and interactions between the cells and the mucoderm® matrix, cells (30,000 cells/well) were cultured on the mucoderm® samples in 24-well plates and stained with cytogreen fluorescent dye (Cyto-ID™ Green; Enzo Life Sciences, Farmingdale, NY, USA) at different points of measurement. They were viewed and photographed with an inverted fluorescence microscope (Axiovert 40C/Carl Zeiss, Göttingen, Germany) at magnifications of × 25–400.

3-(4,5-dimethylthiazol-2-yl)-2,5-diphenyl tetrazolium bromide colorimetric cell viability

To examine the cell viability of tested cell lines, a 3-(4,5-dimethylthiazol-2-yl)-2,5-diphenyl tetrazolium bromide colorimetric assay (MTT) (Sigma, Steinheim, Germany) was performed. Tetrazolium bromide is reduced to formazan by viable cells. Formazan can be measured after cell lysis photometrically at 550 nm.

For the MTT assay, blanked discs of the membrane (diameter 6 ± 0.1 mm) were transferred into 48 wells of 96-well plates. Remaining 48 wells were used as the tissue culture polystyrene surface (TCPS) control group. Subsequently, cells of the respective cell line were transferred into the 96 wells (each 10,000 cells/well). Cell viability was measured at three points of time after 3, 6 and 9 d of cell growing with a Synergy HT Multi-Mode Microplate Reader (corresponding setting: absorbance; BioTek Instruments, Winooski, VT, USA). For each tested cell line and for each of the three points of measurement, respectively 48 wells with mucoderm® matrices and 48 wells of controls were prepared. After the triplicate performance of the MTT assay, in total, for each tested cell line, respectively 432 wells with mucoderm® matrices and 432 controls were used.

PrestoBlue® cell viability

PrestoBlue® assay (Invitrogen, Life Technologies GmbH, Darmstadt, Germany) was used to assess the influence of the collagen membrane on the viability of the tested cell lines. This assay contains a fluorometric growth indicator and is based on the detection of metabolic mitochondrial activity. PrestoBlue® Cell Viability Reagent (Invitrogen) is a soluble, nontoxic blue stain incorporated by cells and reduced to a red fluorescing stain (resorufin) in accordance with their proliferative activity. This test allows visualization of cell viability by monitoring the catalytic effects of NADPH/NADH-dependent dehydrogenases within the cells, the concentrations of which are directly proportional to cell proliferation. In proliferating cells, the ratio between NAD(P)H/NAD(P) is shifted in the direction of NAD(P)H. Ninety-six-well plates were prepared similar to the MTT assay (each 10,000 cells/well). At 12–84 h (12, 18, 32, 42, 58, 72 and 84 h) after applying 10% PrestoBlue®, the color change induced by the reduction of resazurin to resorufin was measured at a wavelength of 560/20 and 620/40 nm with a Synergy HT Multi-Mode Microplate Reader (corresponding setting: fluorescence; BioTek Instruments, Winooski, VT, USA) and analyzed with Gen5 (BioTek Instruments, Bad Friedrichshall, Germany). Logarithmic signals were converted to a linear scale and expressed as relative fluorescence units. For each tested cell line, respectively 48 wells with mucoderm® matrices and 48 wells of controls were prepared. After the triplicate performance of the PrestoBlue® assay, in total, for each tested cell line, respectively 144 wells with mucoderm® matrices and 144 controls were used.

ToxiLight® cytotoxicity assay

The cytotoxic potential of the employed collagen membrane was investigated using the ToxiLight® BioAssay Kit (Lonza Rockland, Inc., Rockland, ME, USA). The ToxiLight® BioAssay is a nondestructive, bioluminescent cytotoxicity assay that quantitatively measures the release of adenylate kinase (AK) from damaged cells. AK, a phosphotransferase enzyme, plays an important role in cellular energy homeostasis catalyzing the interconversion of adenine nucleotides. AK is present in all cells. A loss of cell integrity due to cell damage results in its release from the cell cytoplasm. *In vitro*, the measurement of AK release within the cell medium allows the accurate and sensitive determination of cytotoxicity and cytolysis. Ninety-six-well plates were prepared similar to the MTT assay (each 25,000 cells/well). After different points of time (24, 48, 72, 96 and 120 h), the supernatant was mixed

with ToxiLight® agent. After a short incubation time, the emitted light intensity was measured using a Synergy HT Multi-Mode Microplate Reader (corresponding setting: luminescence; BioTek Instruments, Winooski, VT, USA). Logarithmic signals were converted to a linear scale and expressed as relative luminescence units. Cells on TCPS served as controls. For each tested cell line, respectively 48 wells with mucoderm® matrices and 48 wells of controls were prepared. After the triplicate performance of the ToxiLight assay, in total, for each tested cell line, respectively 144 wells with mucoderm® matrices and 144 controls were used.

Mouse experimental design

All animal experiments were approved by the local ethical committee. In total, six female euthymic nude mice (Crl:SKH1-hr; Charles River Laboratories Inc., Wilmington, MA, USA) aged 6–8 wk and weighing each between 26 and 28 g, were used.

The mice acclimated for 14 d before treatment. They were housed in a 12 h light–dark cycle at 22°C with water and food *ad libitum*. For the mucoderm® implantation the mice were anesthetized using a narcotic mixture of ketamin (ketamin-ratiopharm®; ratiopharm GmbH, Ulm, Germany), xylazin (Rompun®; Bayer Vital GmbH, Leverkusen, Germany) and sodium chloride solution (250 µL each per animal) by intraperitoneal injection, using a 26-gauge needle. For harvesting, the animals were killed with an overdose of the narcotic mixture. After the first 2 wk of acclimatization, two mucoderm® matrices (diameter 8.0 mm, ± 0.1 mm) were implanted subcutaneously right and left alongside the dorsal midline of each mouse. After 21 d *in situ*, the mice were killed (Fig. 1).

Tissue sampling and histology

The mucoderm® matrices and the surrounding tissues were dissected from the back and placed in 10% formalin at room temperature for 2 d. From each specimen, respectively three microslides from the center and the border areas for each of the three different stainings: hematoxylin and eosin (H&E), CD31 and Ki-67 were prepared. Slides for histology were obtained and H&E stained. Microvessel densities and proliferation densities were determined in anti-CD31- and anti-Ki-67-stained frozen sections. Immunohistochemical staining of endothelial cells was performed using a monoclonal antibody against CD31 (BD Biosciences Pharmingen, Heidelberg, Germany). Immunohistochemical staining of proliferating cells was performed using a monoclonal antibody against Ki-67 (DakoCytomation GmbH, Hamburg, Germany). Antibody binding was visualized via a three-step staining procedure using a biotinylated polyclonal antirat IgG secondary antibody (DakoCytomation GmbH) and the streptavidin horseradish peroxidase reaction together with the DAB detection system. For negative controls of the immunohistochemistry, slides of the mucoderm® matrices were stained with the antibody dilution solution without a primary antibody, which is normally used to attenuate the primary antibody against CD31 and Ki-67 (Antibody Diluent; DakoCytomation GmbH).

Using a Leica MS 5 tripod (Leica Microsystems, Wetzlar, Germany) equipped with a JVC KY-F75U C mount digital camera (JVC, Yokohama, Japan), all sections were scanned on a light panel LP-200 cold cathode light panel (Universal Electronics Industries, Hong Kong) and stored and analyzed using the Diskus morphometry software (Diskus 4.50; Hilgers, Königswinter, Germany).

Data analysis

Comparisons were analyzed by ANOVA (*post-hoc* test: Tukey) (SPSS version 17.0). $p < 0.05$ was considered to be statistically significant.

In each assay (MTT, PrestoBlue, ToxiLight) and each cell line, all subgroups (control, mucoderm®) of each point of measurement were compared with each other point of measurement (in totally: MTT assay six subgroups; PrestoBlue assay 14 subgroups; ToxiLight assay 10 subgroups). Continuous variables were expressed as mean values with standard deviations in the vertical bar charts. Differences are given for comparison between the mucoderm® and the control group for the particular point of measurement.

Results

Scanning electron microscopy and interferometric images

SEM examination of porcine collagen matrix is presented in Fig. 2. The scaffold presents a monolayered matrix with uniform and well-regulated structures (Fig. 2A). The cross-section in higher magnification revealed that this matrix consisted of large parallel sheets of lowly compressed collagen fibers (Fig. 2B). This high-porosity spongious layer of the matrix, created to facilitate tissue and microvessel

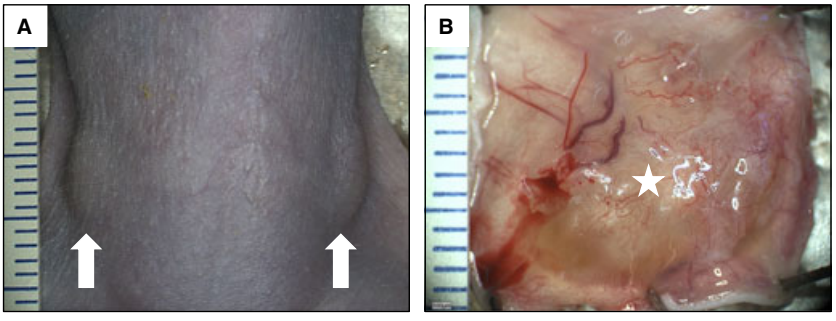

Fig. 1. Two subcutaneously implanted mucoderm® matrices on the left and on the right side under the dorsal skin of a nude mouse *in situ* (white arrows) (A) and a dissected mucoderm® matrix after explantation with the overlying skin (white asterisk) (B).

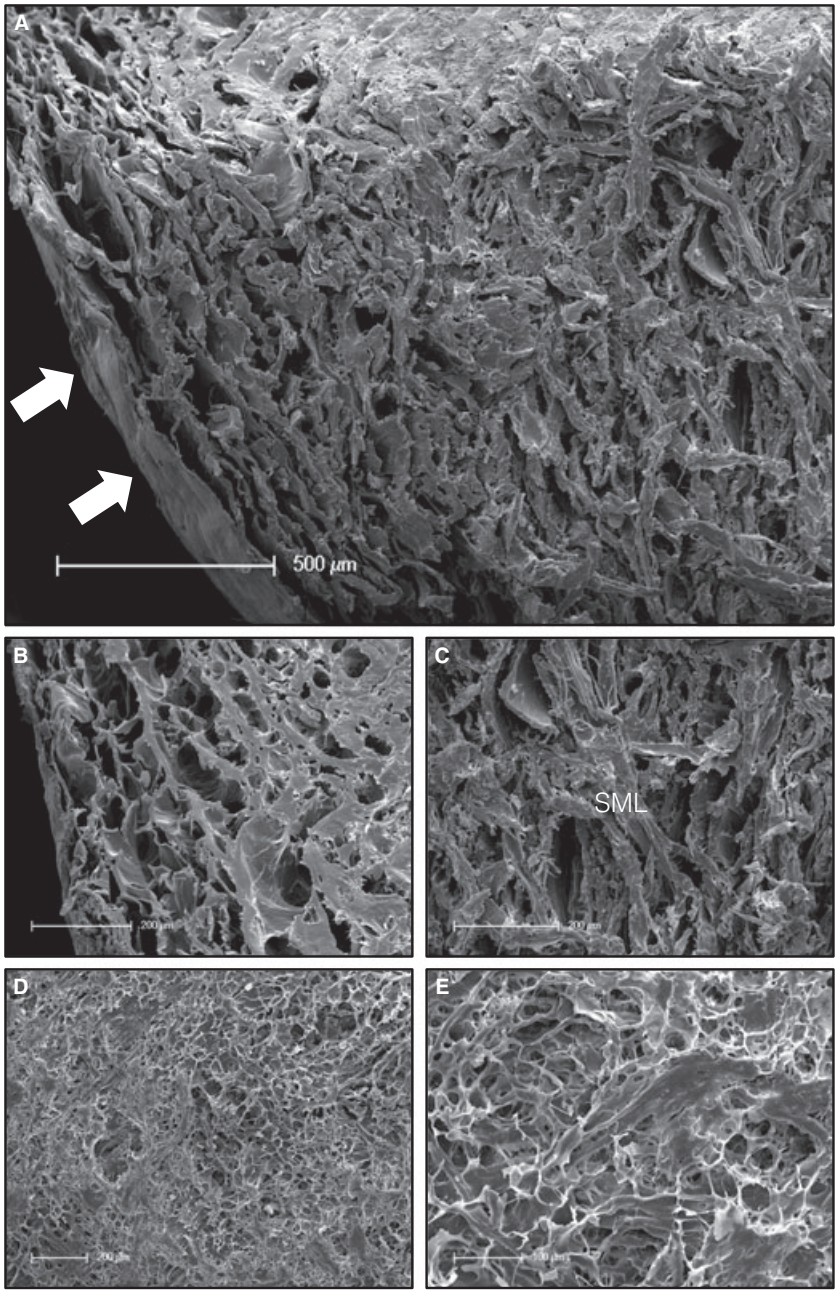

Fig. 2. Scanning electron microscopy of the mucoderm® matrix, showing a low magnification (50-fold) cross-section with the surface layer marked with white arrows (A). Additionally, the cross-section in higher magnification (100-fold) (B) demonstrating the high-porosity spongious monolayer (SML) of the matrix (C). The surface layer of the matrix in a high magnification (100-fold and 200-fold) is shown in (D) and (E).

ingrowth, has a surface and structure that is highly porous and has diffusely packed collagen fibers (Fig. 2C). In addition, the surface layer of the matrix in a low (Fig. 2D) and high magnification (Fig. 2E) revealed the morphology of the monolayered matrix. It demonstrated low porosity of the surface layer, which is suitable for tissue and microvessel ingrowth in a high density. The 3D microscopy and 3D structural analysis of the surface layer (Fig. 3) demonstrated roughness parameters between 0.0 and 225.6 µm and clarified that this structure has been designed to facilitate a high cell adherence, proliferation and migration ability on the mucoderm® matrix.

MTT and PrestoBlue® analysis

In the MTT assay a statistically significant increase of cell viability could be detected for all tested cell lines at each point of measurement (each $p < 0.001$) with exception of the particular points of measurement after 3 d for gingival fibroblasts and keratinocytes (each $p > 0.05$; Fig. 4). For endothelial cells, osteoblasts, fibroblasts and keratinocytes at each point of measurement after 6–9 d a statistically significant increase of cell viability could be detected (each $p < 0.05$). In particular, the tested collagen matrix seems to induce a strong increase in cell viability after 9 d in comparison to osteoblasts and endothelial cells on gingival fibroblasts and keratinocytes, which is important for soft tissue building and regeneration.

In the PrestoBlue® assay a statistically significant increase of cell viability could be detected for all tested cell lines at each point of measurement (each $p < 0.05$) with the exception of particular points of measurement after 12–18 h for all tested cell lines (each $p > 0.05$; Fig. 5). For endothelial cells, osteoblasts, fibroblasts and keratinocytes at each point of measurement from 32 to 84 h, a statistically significant increase of cell viability could be detected (HGF $p < 0.01$; HOB, HUVEC, HOK each $p < 0.001$).

ToxiLight® analysis

Using the ToxiLight® assay, no statistically significant increase of AK release could be detected for all tested cell lines at each point of measurement from 24 to 120 h (each $p > 0.05$; Fig. 6). For endothelial cells and keratinocytes at the particular points of measurement after 120 h, an increase of AK release could be detected for the mucoderm® matrix in comparison to the TCPS that did not become statistically significant (each $p > 0.05$).

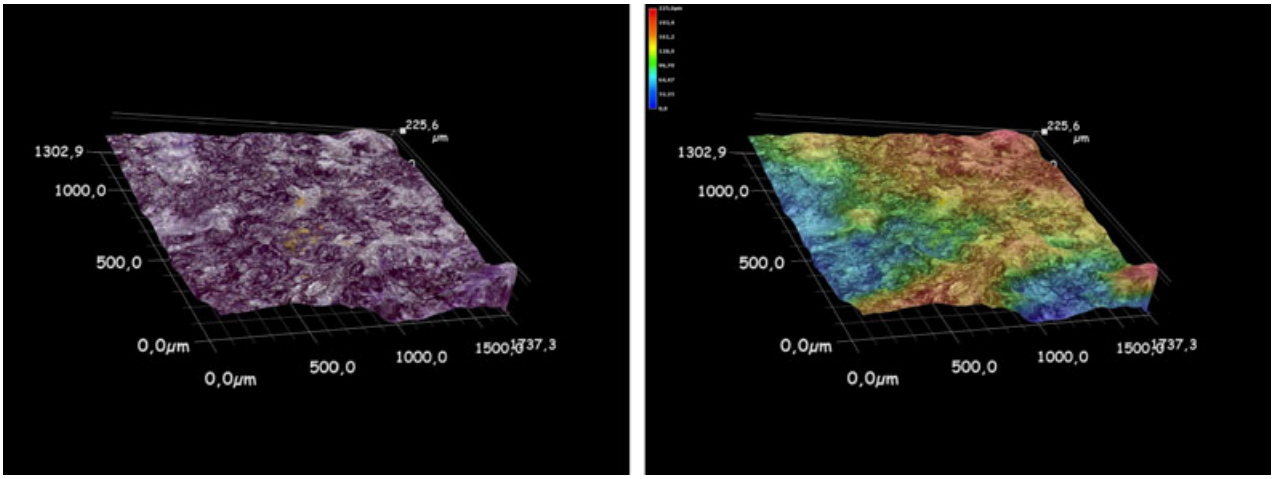

Fig. 3. Three-dimensional microscopy of the surface layer of a 1.302 × 1.737 mm large area (roughness parameters 0.0–225.6 µm).

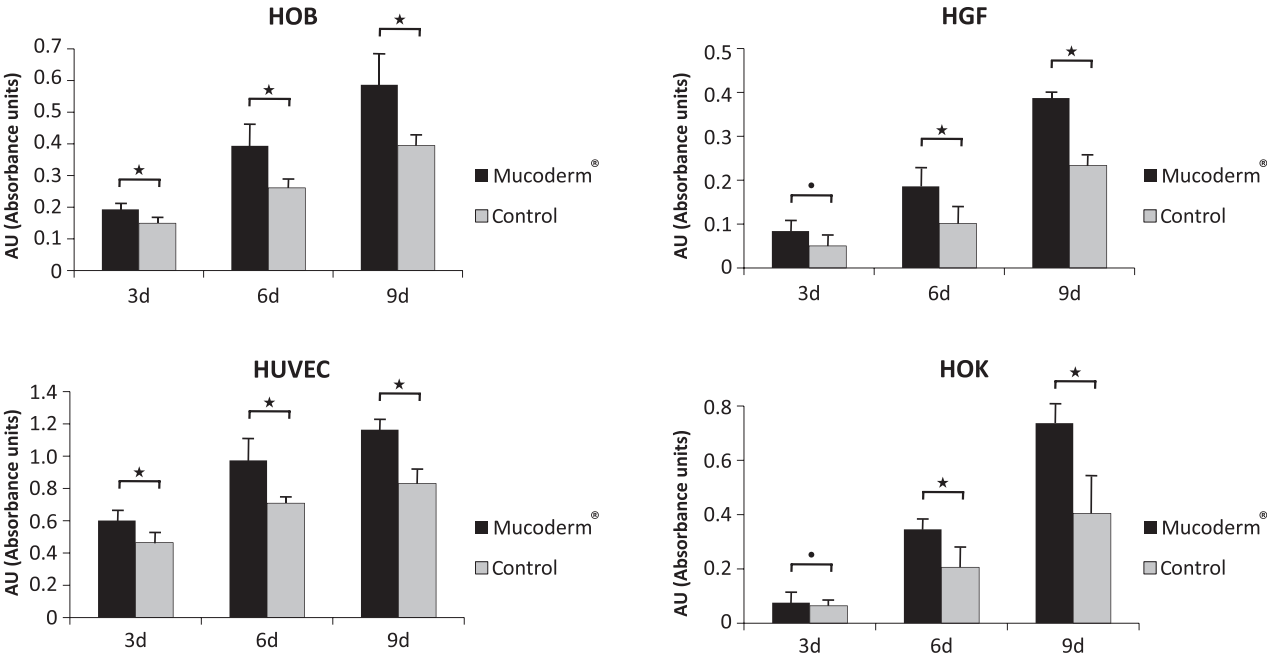

Fig. 4. MTT assay. Cell viability test for human osteoblast-like (HOB) cells, human gingival fibroblasts (HGF), human umbilical vein endothelial cells (HUVEC) and human oral keratinocytes (HOK) on the mucoderm® matrix. *x*-axis = point of measurement; *y*-axis = cell viability measured in absorbance units (AU). Asterisks = statistically significant ($p < 0.05$); circles = statistically non-significant ($p > 0.05$).

Cell morphology and distribution on the porcine acellular dermal matrix

The morphologic appearance and density of fibroblasts on the PADM surface is indicative of good adherence of HGF to the PADM surface. After 24 h (Fig. 7A–C), the overview (Fig. 7A) revealed a low cellular density on mucoderm® matrix at a defined local area. The overview (Fig. 7B and 7C) exhibited a normal cell population with a subconfluent cell layer and well-spread cells. Normal cellular morphologies consisting of fully spread cells with development of lamellipodias and filopodias could be observed.

After 5 d (Fig. 7D–F) and 14 d (Fig. 7G–I), multiple cell areas could be detected as a clear indicator for increased cellular homeostasis and a high proliferation and migration ability. In addition, at higher magnification (Fig. 7E,F and 7H,I) close cell contacts could be demonstrated as an indicator for high adherence on the matrix.

Histological observation

The initial analysis of PADM explants consisted of careful examination of

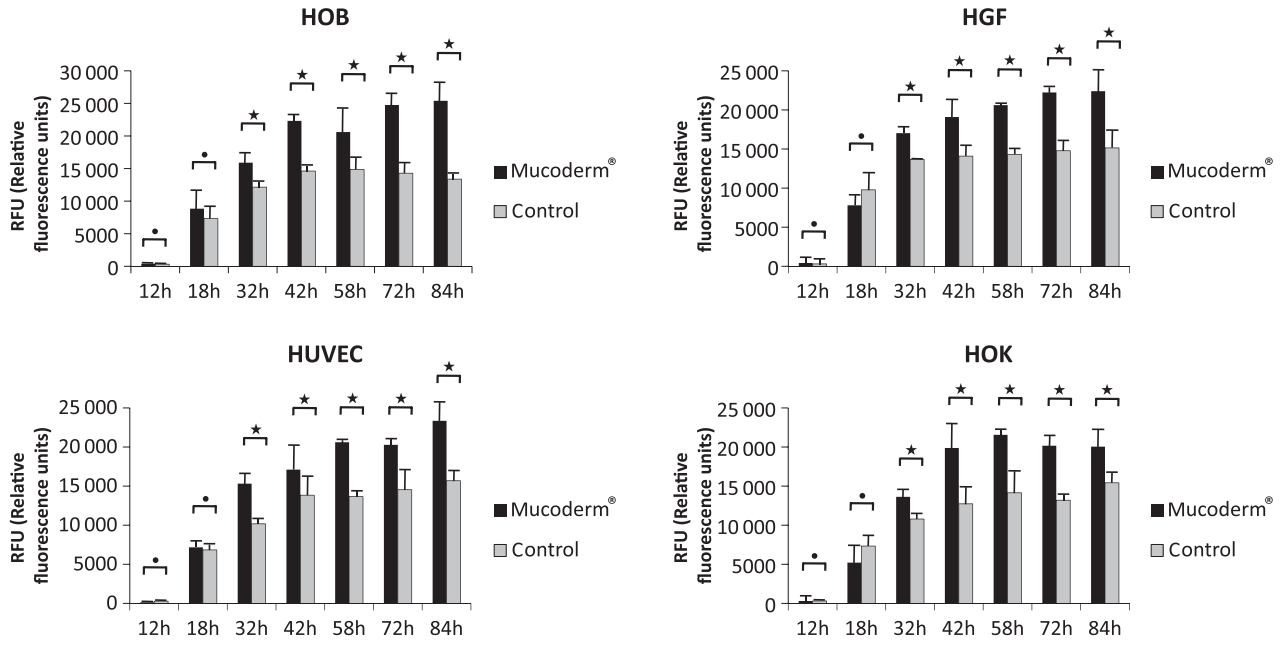

Fig. 5. PrestoBlue® assay. Cell viability test for human osteoblast-like (HOB) cells, human gingival fibroblasts (HGF), human umbilical vein endothelial cells (HUVEC) and human oral keratinocytes (HOK) on the mucoderm® matrix. *x*-axis = point of measurement; *y*-axis = cell viability measured in relative fluorescence units (RFU). Asterisks = statistically significant ($p < 0.05$); circles = statistically non-significant ($p > 0.05$).

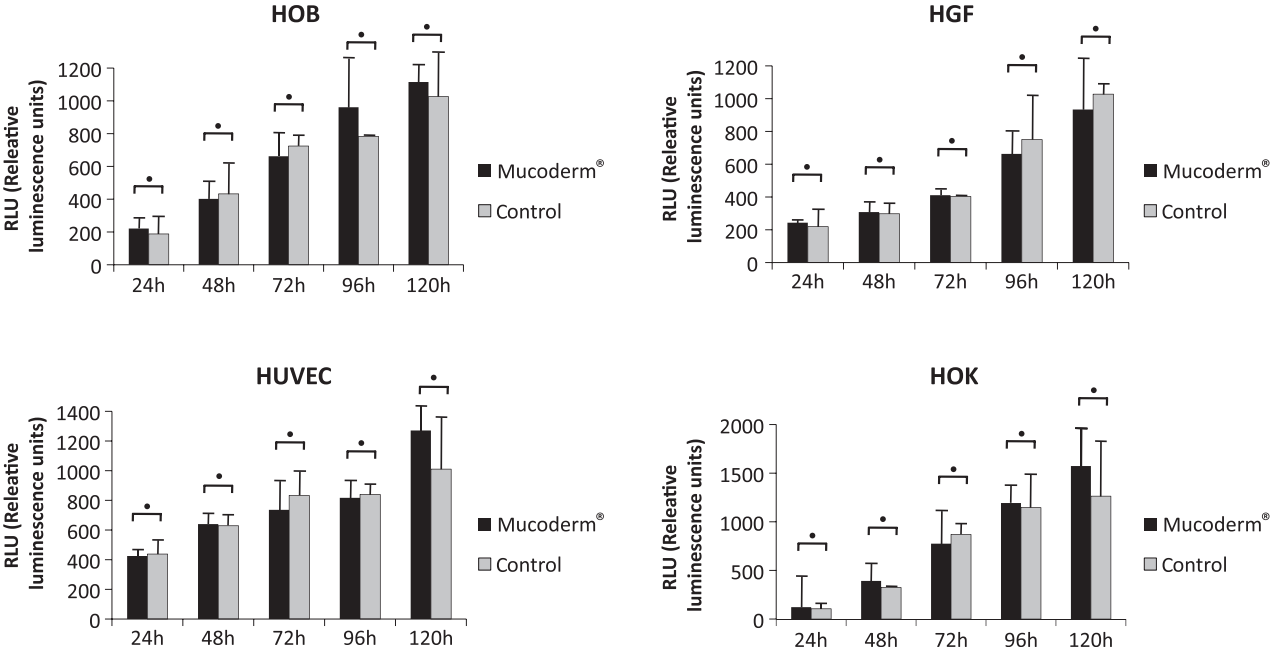

Fig. 6. ToxiLight® assay. Cytotoxicity test for human osteoblast-like (HOB) cells, human gingival fibroblasts (HGF), human umbilical vein endothelial cells (HUVEC) and human oral keratinocytes (HOK) on the mucoderm® matrix. *x*-axis = point of measurement; *y*-axis = cytotoxicity measured in relative luminescence units (RLU). Circles = statistically non-significant ($p > 0.05$).

H&E-stained cross-sections. At 21 d after implantation, H&E staining (Fig. 8A–C) demonstrated in the low magnification the mucoderm® matrix (white asterisk) as well as the interface between the host tissue, the spongy monolayer and the subcutaneous tissue (Fig. 8A). Figure 8B,C show the interface between the matrix and the subcutaneous tissue with multiple cells penetrating the monolayer (white arrows) (Fig. 8C).

CD31 immunohistochemical staining (Fig. 8D–F) for microvessel detection demonstrated a high and sufficient

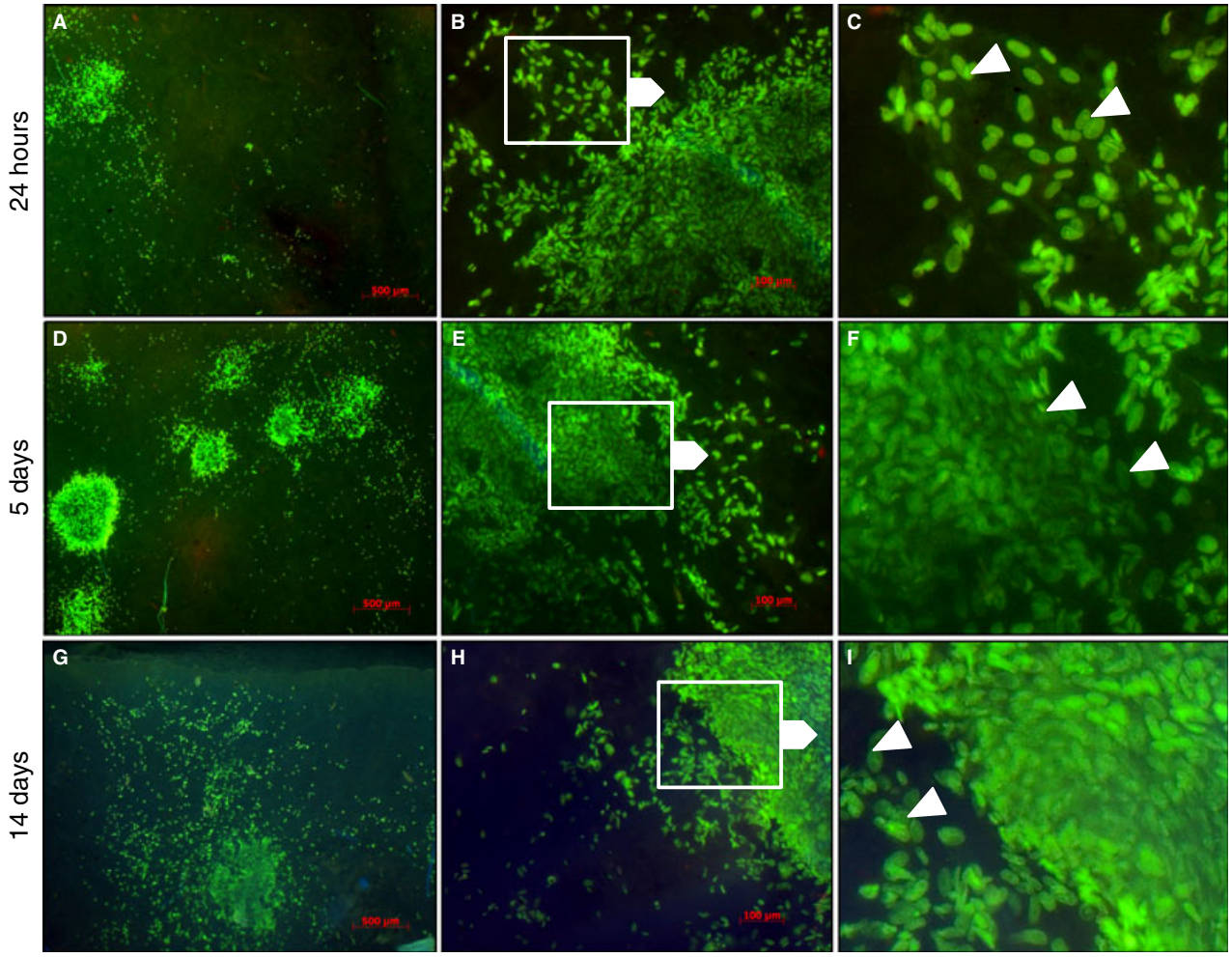

Fig. 7. Visualization of stained (CytoGreen®) gingival fibroblasts (GF) seeded on mucoderm® matrix after 24 h (A, B, C), 5 d (D, E, F) and 14 d (G, H, I). (A, D, G) Overview in a lower magnification (10-fold) at different points of visualization. Overview and more detailed analysis of cellular phenotypes in a higher magnification (20-fold) (B, E, H) with increased apertures of interesting areas on the right (C, F, I). Green fluorescence demonstrates the cell nuclei, cell membrane and parts of the cytoplasm. Intercellular adherences and cell contacts are demonstrated with white arrows (C, F, I).

revascularization of the matrix with multiple newly formed and insprouting blood vessels (white arrows) (Fig. 8F).

Ki-67 immunohistochemical staining (Fig. 8G–I) for the detection of proliferating cells revealed a high proliferation rate in the mucoderm® matrix (white asterisk) as an indicator for the high mitosis rate and a high proliferation and migration ability of the cells in the matrix (white arrows) (Fig. 8I).

Discussion

The present study was designed to evaluate the biological properties of a novel PADM by seeding this matrix with HGF, HOB, HUVEC and HOK. In addition, the *in vivo* tissue reactions were tested histologically after subcutaneous implantation in mice. The results of our *in vitro* cell–matrix interactions demonstrated that the properties of this novel PADM supported metabolic activity and proliferation of HGF, osteoblasts, endothelial cells and oral keratinocytes. The MTT, PrestoBlue® and ToxiLight® assays demonstrated no interference of the novel PADM with cell viability over time. It is well known that cell adhesion and subsequent proliferation and differentiation are influenced by surface characteristics of the 3D matrices. In the present study, both surface and cross-sectional SEM demonstrated high porosity and high interconnectivity of the matrix. Indeed, the investigation of biodegradable synthetic collagen matrices as a cell carrier demonstrated lower cell migration on matrices with a dense structure compared to a scaffold with a loose fibrillar structure (8). These findings are also congruent with our previous observations, which demonstrated a lower proliferation rate of HGF in matrices with a dense structure (9). However, although the present study showed that cells adhered and spread on the dermal matrix surface, the internal distribution of these cells was not evaluated. Therefore, it cannot be excluded that cell proliferation and migration took place mostly on its outer surface.

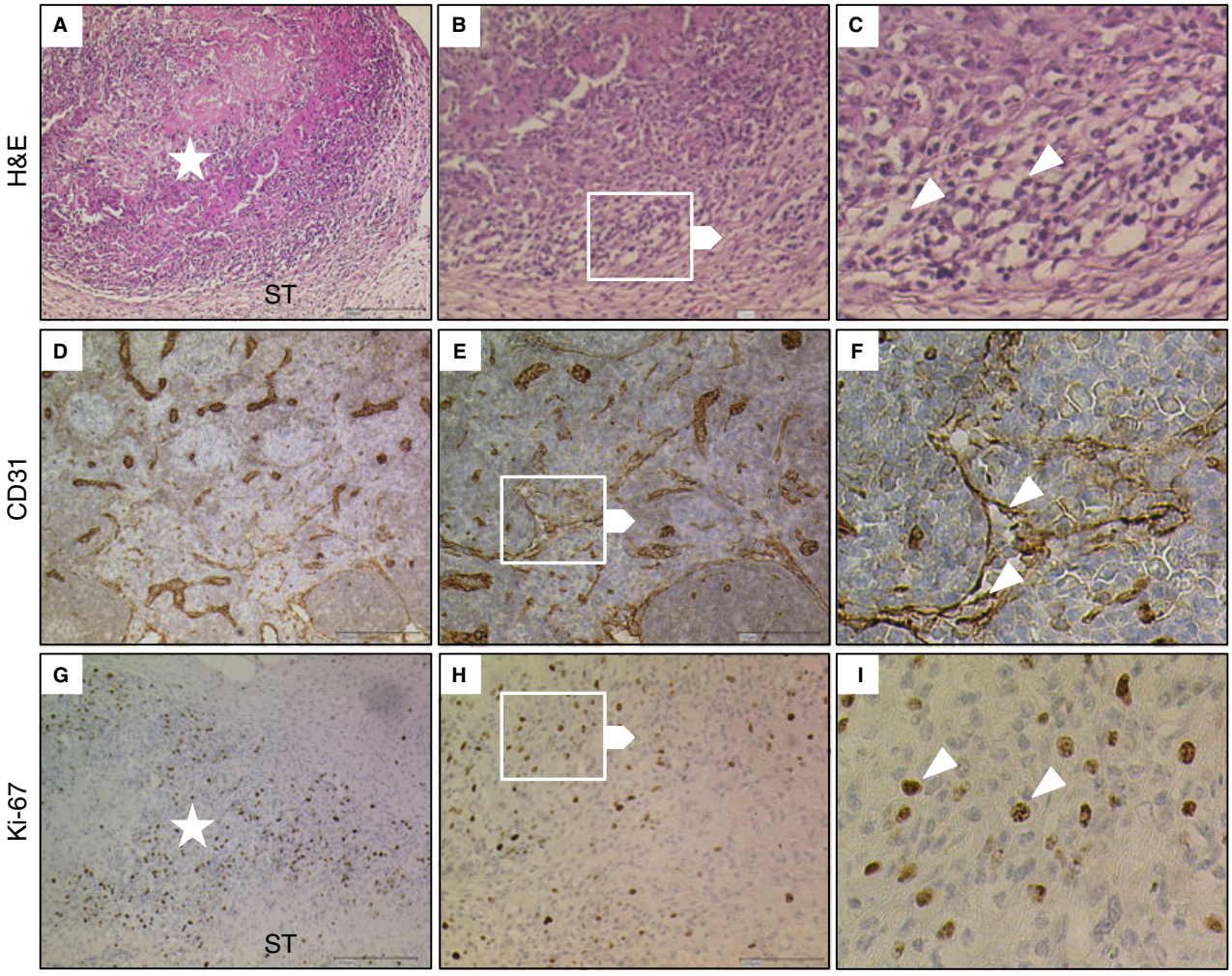

Fig. 8. Twenty-one days post-implantation histological images showing cross-sections of the mucoderm® matrix with H&E (A–C), CD31 (D–F) and Ki-67 (G–I) staining. Overview in a lower magnification (10-fold) (A, D, G) and Overview and more detailed analysis of cellular in a higher magnification (20-fold) (B, E, H) with increased apertures of interesting areas on the right (C, F, I). White asterisks demonstrate the mucoderm® matrix. White arrows demonstrate immigrated cells in H&E staining (C), endothelial cells in CD31 staining and proliferating cells in Ki-67 staining (I). H&E, hematoxylin and eosin; ST, subcutaneous tissue.

Thus, Rodrigues *et al*. (10), evaluating fibroblast seeding on an ADM surface, observed good conditions for cell adhesion and spreading on the matrix, but reduced migration of cells through the matrix.

The beneficial effect of fibroblast seeding on ADM is also supported by *in vivo* data. A preliminary study (11) found that the addition of gingival fibroblasts to the matrix enhanced vascularization *in vivo* during the early stages of healing. More recently, Jhaveri *et al*. (12) demonstrated no significant differences between ADM seeded with autologous gingival fibroblasts and subepithelial connective tissue autograft for the treatment of Miller class I and II recession defects.

In this report, porcine 3D collagen matrix was shown to support human osteoblast growth. This observation is supported by previous data demonstrating that ADM has no negative effects on the growth of osteoblast-like cells (13). The surface characteristic of a scaffold structure is well known as a key factor to govern cell response. Thus, it could be shown that surface roughness influences osteoblastic cells depending on their maturation state (14).

The present findings suggest that the PADM could be used to synthesize a tissue-engineered bone tissue scaffold. A previous study has already reported success with a periosteum-like material composed of ADM and osteoblasts or mesenchymal stem cells (15). Recently, Zhao *et al*. (16) described the preparation of a bone tissue scaffold consisting of porous hydroxyapatite collagen and PADM for the purpose of treating bone defects.

As the PADM has no blood vessels or cells, its incorporation into surrounding tissues largely depends on cell and blood vessel infiltration. The formation of new capillaries requires activation, migration and proliferation

of endothelial cells from preexisting vessels in the process of angiogenesis (17). In the present study, we investigated the effects of PADM on primary endothelial cells. The HUVEC culture is a well-established *in vitro* cell model for molecular imaging of angiogenesis (18). Our data demonstrated that PADM is capable of supporting growth of HUVECs. This observation is in accordance with Zhang *et al*. (19), who reported a significantly increased proliferation of HUVECs on PADM. Moreover, the authors showed that HUVECs seeded on PADM stimulated the formation of capillary-like networks *in vivo*.

Our studies of human keratinocytes in cell culture revealed that PADM supported human keratinocyte proliferation and cell survival. These findings are consistent with several reports in the literature. Using a cell culture assay, Zajicek *et al*. (20) demonstrated that acellular porcine dermis is an appropriate substrate for keratinocyte attachment, growth and differentiation. Izumi *et al*. (21), preparing an oral mucosa equivalent consisting of autogenous oral keratinocytes and cadaveric human dermis, observed that keratinocytes of the equivalent appeared to be in a more active and proliferative state than native keratinized mucosa.

Previous studies evaluating dermal–epidermal composites, used fibroblasts as a feeder layer to enhance adherence of keratinocytes to ADM and promote growth and proliferation on the surface of ADM (22,23). Indeed, fibroblasts can secrete various cytokines, growth factors and extracellular matrix components, which promote proliferation of epithelial cells (24). However, our results imply that the PADM can promote proliferation of keratinocytes without the need of a fibroblast feeder layer. This may be attributed, at least in part, to the biological structure of the matrix, which is similar to the normal dermis and thus favorable for differentiation of keratinocytes.

The promising results obtained *in vitro* are further in corroboration with our *in vivo* findings. Thus, examination of tissue specimens after healing in subcutaneous pockets demonstrated active host cell proliferation within the matrix and extensive ingrowth of vessels after 21 d. Microvessel ingrowth is absolutely essential to ensure perfusion of an implanted matrix, resulting in sufficient incorporation of the matrix, to prevent avascular wound infections and to ensure high-quality wound healing.

Moreover, the histological findings showed that the matrix was well-tolerated without an immunological or foreign body response. These findings are supported by Eppley (25), who demonstrated in an *in vivo* animal model that revascularization of a single layer acellular human dermis occurred rapidly and was essentially complete by 14 d after surgery. Similarly, Wong *et al*. (4) evaluating *in vivo* the revascularization of human ADM, observed that after 14 d mature $CD31^+$ microvessels were present throughout the matrix. However, the question whether complete through-and-through revascularization has been achieved in the present study cannot be answered. Moreover, one might speculate that differences may exist in the tissue reaction between porcine and human acellularized dermis. The morphological and functional similarities of porcine and human skin have been reported to be comparable (26). Hoyama *et al*. (27), showed histologically that human and porcine acellular dermal tissue are both well-tolerated when implanted in the subcutaneous tissue of rats. Moreover, an increased number of vessels inside the implants and surrounding tissues of the porcine graft could be observed 6 mo postoperatively. In contrast, Richter *et al*. (28) demonstrated *in vivo* a significantly greater soft tissue ingrowth and microvascular density in human-based dermis compared to porcine-based dermis. Using a subcutaneous murine model, Ghanaati *et al*. (29) showed that the central parts of a bilayered porcine matrix became vascularized between days 30 and 60. The authors concluded that the compact layer of the matrix inhibited cell infiltration for the first 30 d. These findings further support our assumption that the natural biological structure of the dermis plays an important role in vascularization and tissue incorporation.

Finally, one must be cautious in the interpretation of results obtained by using *in vitro* and *in vivo* animal experimental studies, as they cannot recreate the complex biological system that occurs in the human oral cavity.

In summary, the present results provide evidence *in vitro* that PADM can promote growth and proliferation of HGF, osteoblasts, endothelial cells and oral keratinocytes. These findings also indicate that the PADM seeded with the different oral cell lines may serve as a potential system for tissue engineering purposes. Furthermore, it was shown *in vivo* that PADM is capable of significant revascularization of its collagen structure in the early healing period. Overall, the results suggest that PADM is a promising substitute for autogenous soft tissue grafts in periodontal plastic surgery. However, future studies are needed to clarify if these findings can be transferred to a clinical setting.

Acknowledgements

This study was supported by MAIFOR (University of Mainz, science support).

References

1. Zucchelli G, Amore C, Sforza NM, Montebugnoli L, De Sanctis M. Bilaminar techniques for the treatment of recession-type defects. A comparative clinical study. *J Clin Periodontol* 2003;**30**: 862–870.
2. Cairo F, Pagliaro U, Nieri M. Treatment of gingival recession with coronally advanced flap procedures: a systematic review. *J Clin Periodontol* 2008;**35**:136–162.
3. Chambrone L, Sukekava F, Araujo MG, Pustiglioni FE, Chambrone LA, Lima LA. Root-coverage procedures for the treatment of localized recession-type defects: a Cochrane systematic review. *J Periodontol* 2010;**81**:452–478.
4. Wong AK, Schonmeyr B, Singh P, Carlson DL, Li S, Mehrara BJ. Histologic analysis of angiogenesis and lymphangiogenesis in acellular human dermis. *Plast Reconstr Surg* 2008;**121**:1144–1152.
5. Gapski R, Parks CA, Wang HL. Acellular dermal matrix for mucogingival surgery: a meta-analysis. *J Periodontol* 2005;**76**:1814–1822.

6. Jepsen K, Jepsen S, Zucchelli G *et al*. Treatment of gingival recession defects with a coronally advanced flap and a xenogeneic collagen matrix: a multicenter randomized clinical trial. *J Clin Periodontol* 2013;**40**:82–89.
7. Schlee M, Ghanaati S, Willershausen I, Stimmlmayr M, Sculean A, Sader RA. Bovine pericardium based non-cross linked collagen matrix for successful root coverage, a clinical study in human. *Head Face Med* 2012;**8**:6.
8. Hillmann G, Steinkamp-Zucht A, Geurtsen W, Gross G, Hoffmann A. Culture of primary human gingival fibroblasts on biodegradable membranes. *Biomaterials* 2002;**23**:1461–1469.
9. Kasaj A, Reichert C, Götz H, Röhrig B, Smeets R, Willershausen B. In vitro evaluation of various bioabsorbable and nonresorbable barrier membranes for guided tissue regeneration. *Head Face Med* 2008;**4**:22.
10. Rodrigues AZ, Oliveira PT, Novaes AB Jr, Maia LP, Souza SL, Palioto DB. Evaluation of in vitro human gingival fibroblast seeding on acellular dermal matrix. *Braz Dent J* 2010;**21**:179–189.
11. Novaes AB Jr, Marchesan JT, Macedo GO, Palioto DB. Effect of in vitro gingival fibroblast seeding on the in vivo incorporation of acellular dermal matrix allografts in dogs. *J Periodontol* 2007;**78**:296–303.
12. Jhaveri HM, Chavan MS, Tomar GB, Deshmukh VL, Wani MR, Miller PD Jr. Acellular dermal matrix seeded with autologous gingival fibroblasts for the treatment of gingival recession: a proof-of-concept study. *J Periodontol* 2010;**81**:616–625.
13. Liu M, Wang SA, Mo AC, Meng Y, Hu J, Li XY. Study on the microstructure of acellular dermal matrix and its biocompatibility with MG 63 osteoblast-like cells. *Hua Xi Kou Qiang Yi Xue Za Zhi* 2008;**26**:129–132.
14. Lohmann CH, Bonewald LF, Sisak MA *et al*. Maturation state determines the response of osteogenic cells to surface roughness and 1,25-dihydroxyvitamin D3. *J Bone Miner Res* 2000;**15**: 1169–1180.
15. Schönmeyr B, Clavin N, Avraham T, Longo V, Mehrara BJ. Synthesis of a tissue-engineered periosteum with acellular dermal matrix and cultured mesenchymal stem cells. *Tissue Eng Part A* 2009;**15**:1833–1841.
16. Zhao H, Wang G, Hu S *et al*. In vitro biomimetic construction of hydroxyapatite-porcine acellular dermal matrix composite scaffold for MC3T3-E1 preosteoblast culture. *Tissue Eng Part A* 2011;**17**:765–776.
17. Carmeliet P. Angiogenesis in health and disease. *Nat Med* 2003;**9**:653–660.
18. Kim DH, Choe YS, Jung KH, Lee KH, Choi Y, Kim BT. Synthesis and evaluation of 4-[(18)F]fluorothalidomide for the in vivo studies of angiogenesis. *Nucl Med Biol* 2006;**33**:255–262.
19. Zhang X, Yang J, Li Y *et al*. Functional neovascularization in tissue engineering with porcine acellular dermal matrix and human umbilical vein endothelial cells. *Tissue Eng Part C Methods* 2011;**17**: 423–433.
20. Zajicek R, Mandys V, Mestak O, Sevcik J, Königova R, Matouskova E. Human keratinocyte growth and differentiation on acellular porcine dermal matrix in relation to wound healing potential. *Sci World J* 2012;**2012**:727352.
21. Izumi K, Terashi H, Marcelo CL, Feinberg SE. Development and characterization of a tissue-engineered human oral mucosa equivalent produced in a serum-free culture system. *J Dent Res* 2000;**79**:798–805.
22. Xiao SC, Zhu SH, Li HY, Yang J, Xia ZF. A new strategy of using keratinocytes for skin graft: animal experimental study of keratinocyte suspension combined with the dermal substitutes. *Eur Surg Res* 2009;**43**:1–7.
23. Pellegrini G, Ranno R, Stracuzzi G *et al*. The control of epidermal stem cells (holoclones) in the treatment of massive full-thickness burns with autologous keratinocytes cultured on fibrin. *Transplantation* 1999;**68**:868–879.
24. Werner S, Krieg T, Smola H. Keratinocyte-fibroblast interactions in wound healing. *J Invest Dermatol* 2007;**127**: 998–1008.
25. Eppley B. Experimental assessment of the revascularization of acellular human dermis for soft-tissue augmentation. *Plast Reconstr Surg* 2001;**107**:757–762.
26. Meyer W, Schwarz R, Neurand K. The skin of domestic mammals as a model for the human skin, with special reference to the domestic pig. *Curr Probl Dermatol* 1978;**7**:39–52.
27. Hoyama E, Schellini SA, Marques ME, Rossa R, Padovani CR. A comparison of human and porcine acellular dermal tissues in the subcutaneous space of a rat model. *Orbit* 2005;**24**:249–255.
28. Richter GT, Smith JE, Spencer HJ, Fan CY, Vural E. Histological comparison of implanted cadaveric and porcine dermal matrix grafts. *Otolaryngol Head Neck Surg* 2007;**137**:239–242.
29. Ghanaati S, Schlee M, Webber MJ *et al*. Evaluation of the tissue reaction to a new bilayered collagen matrix in vivo and its translation to the clinic. *Biomed Mater* 2011;**6**:015010.